

RESEARCH ARTICLE

10.1002/2016SW001446

Key Points:

- Station-specific models of ionospheric irregularities have been developed
- The inputs include local time, day number of year, $F_{10.7}$ flux, Dst, and AE indices
- Hourly median strengths of ionospheric irregularities are the output

Correspondence to:

P. Mungufeni,
pmungufeni@gmail.com

Citation:

Mungufeni, P., J. B. Habarulema, and E. Jurua (2016), Modeling of ionospheric irregularities during geomagnetically disturbed conditions over African low-latitude region, *Space Weather*, 14, 710–723, doi:10.1002/2016SW001446.

Received 9 JUN 2016

Accepted 8 SEP 2016

Accepted article online 12 SEP 2016

Published online 6 OCT 2016

Modeling of ionospheric irregularities during geomagnetically disturbed conditions over African low-latitude region

Patrick Mungufeni^{1,2}, John Bosco Habarulema^{3,4}, and Edward Jurua¹

¹Department of Physics, Mbarara University of Science and Technology, Mbarara, Uganda, ²Telecommunications/ICT for Development Laboratory of the International Center for Theoretical Physics, Trieste, Italy, ³South African National Space Agency Space Science, Hermanus, South Africa, ⁴Department of Physics and Electronics, Rhodes University, Grahamstown, South Africa

Abstract In this study, station-specific models of ionospheric irregularities over low-latitude African region during geomagnetically disturbed days ($Dst \leq -50$ nT) have been developed. Global Navigation Satellite Systems (GNSS)-derived ionospheric total electron content (TEC) data during 1998–2014 were used. Ionospheric irregularities were represented with the rate of change of TEC index (ROTI). The inputs for the models are the local time, solar flux index, day number of the year, auroral electrojet, and the disturbance storm time indices, while the output is the hourly median ROTI during these given conditions. To develop the models, the ROTI index values were binned based on the input parameters and cubic B splines were then fitted to the binned data. Developed models were validated with independent data over stations within 680 km radius. The models reproduced fairly well the inhibitions and the occurrences of ionospheric irregularities during geomagnetically disturbed days. The models even emulated these patterns in the various seasons, during medium and high solar activity conditions. During validations of the models, the percentages of the number of errors (difference between the observed and the modeled ROTI) < 0.05 total electron content unit, $1\text{TECU} = 10^{16} \text{ el m}^{-2}$ (TECU)/Min at all the stations were all $> 70\%$ and the root-mean-square error were mostly < 0.1 TECU/Min. Furthermore, the correlation coefficients ranged from 0.47 to 0.76.

1. Introduction

Extraordinary fluctuations in the geomagnetic field are generally referred to as geomagnetic storms [Gonzalez *et al.*, 1994]. These fluctuations which are mostly due to the ring current and auroral current flowing in the E region at equatorial and high-latitude regions, respectively, may generate currents in Earth's surface which in turn results in induced currents in telegraph lines, power grids, and enhanced corrosion of pipelines [Benestad, 2006; Akasofu, 2007]. During geomagnetic storms, equatorial zonal electric fields have been frequently observed to differ from their quiet day patterns. According to Blanc and Richmond [1980], these might be due the prompt penetration of high-latitude electric fields and the disturbed dynamo action of storm time winds which produce largest perturbations of electric fields a few hours after the onset of the storm. Fejer and Scherliess [1995] used the extensive radar measurements of F region vertical plasma drifts at the Jicamarca Radio Observatory (magnetic dip 2°N) located in Peru and auroral electrojet (AE) indices to investigate these two mechanisms. They found that when the prompt penetration and disturbed dynamo electric fields occur during daytime, the zonal electric fields over this equatorial region were predominantly eastward and westward, respectively. Due to the eastward electric fields as a result of daytime prompt penetration electric fields, plasma would be lifted to higher altitudes (F region) by $\vec{E} \times \vec{B}$ drifts. After sunset, recombination at such altitudes would be less prevalent. Therefore, daytime prompt penetration electric fields are suitable for creating steep electron density gradients at the bottomside of the raised F layer after sunset. This produces the classical configuration for the Rayleigh-Taylor (RT) instability [Schunk and Nagy, 2009] which is usually associated with the generation of electron density variations in the ionosphere [Sastri *et al.*, 1992; Muella *et al.*, 2009; Li *et al.*, 2009]. These electron density variations are commonly referred to as ionospheric irregularities. The receiver losses of lock on satellites of the Global Navigation Satellite Systems (GNSS) due to small-scale ionospheric irregularities usually result into reduction of the available number of satellites that can be used for position fixing. This increases Geometric Dilution Of Precision (GDOP) and hence increased positioning error [de Paula *et al.*, 2007]. The daytime disturbed dynamo electric fields which creates westwards zonal electric

fields would act contrary to daytime prompt penetration electric fields by pushing down plasma to E region. This condition does not favor triggering of R-T instability and the formation of ionospheric irregularities.

Geomagnetic storms can be quantified by the disturbance storm time (Dst) index which is related to the ring current [Kallenrode, 2003; Akasofu, 2007]. Considering the fact that the magnetic field due to the ring current opposes that of the Earth [Moldwin, 2008], changes in Dst may affect the normal $\vec{E} \times \vec{B}$ drifts (motions of the ionospheric F layer). For instance, negative excursion of Dst during the day might lower the local eastward electric field which in turn reduces upward plasma drifts [Aarons, 1991]. This does not create the necessary conditions for the occurrence of ionospheric irregularities. In particular, the earlier mentioned steep electron density gradient at the bottom side of F layer after sunset which is responsible for the onset of R-T instability. If the large excursion of Dst takes place after sunset and before midnight, the F layer height rise might have occurred during the day. This creates the conditions necessary for generation of ionospheric irregularities [Aarons, 1991]. Therefore, changes in Dst (intensification of the ring current) may result in to generation or inhibition of ionospheric irregularities. The theory that was advanced by Aarons [1991] suggests that when the peak of Dst excursion occurs during 18:00–22:00 LT, there will be little or no effect on the occurrence of ionospheric irregularities that night. When the peak of the excursion of Dst occurs during 00:00–06:00 LT, ionospheric irregularities may occur also around the same time [DasGupta et al., 1985]. Lastly, when the maximum excursion of Dst occurs during 10:00–16:00 LT, ionospheric irregularities may be inhibited on the night that follows.

It now seems to be clear that the inhibition and enhancement of ionospheric irregularities in the low-latitude regions during geomagnetic storms may be related to intensification of the ring current, prompt penetration, and disturbed dynamo electric fields. Most of the available literature regarding modeling of ionospheric irregularities are for quiet time geomagnetic conditions [Scherliess and Fejer, 1999; Abdu et al., 2003; Anderson et al., 2004; Mungufeni et al., 2015]. However, by using a 5 year series of observations at 254 MHz taken at Huancayo, Peru, Aarons [1985] developed analytical equation to yield scintillation excursions as a function of solar flux, magnetic index, local time, and day of the year. Secan et al. [1995] presented an improved Wideband ionospheric scintillation model (WBMOD) that takes geomagnetic activity level as one of its inputs. Their model was developed using data taken from Ancon and Huancayo both in Peru, Manila (Philippines), Kwajalein, and Ascension Islands. Our study aimed to develop empirical models of ionospheric irregularities during geomagnetically disturbed conditions over African low-latitude region. The extensive GNSS-derived ionospheric total electron content (TEC) data during 1998–2014 over Libreville (Gabon) and Malindi (Kenya) have been used to develop separate models. Section 2 describes the data that were used.

2. The Data

The geomagnetically disturbed days were identified by examining the hourly Dst index obtained from the Geomagnetic Data service of Kyoto (<http://swdcwww.kugi.kyoto-u.ac.jp/>). Changes in a day in the zonal electric fields due to a geomagnetic disturbance may have a single corresponding signature on ionospheric irregularities the night that follows. This may be either inhibition when the changes destabilize the necessary conditions for the generation of ionospheric irregularities or occurrence of irregularities. Therefore, a day with any one of the hourly $Dst \leq -50$ nT was considered as geomagnetically disturbed. Gonzalez et al. [1994] and Singh et al. [2004] identified geomagnetic storms when $Dst \leq -50$ nT. With our described method of identifying storm days, a total of 695 days were identified as storm days during 1998–2014.

Figure 1 presents the distribution of the number of storm days per year (blue bars). In the figure, the green and brown bars represent the number of storm days when there were TEC data over Libreville and Malindi, respectively. The total number of storm days when there were TEC data over Libreville and Malindi were 504 and 593, respectively. In sunspot number cycle 23, the years 2007, 2008, and 2009 had low mean $F_{10.7}$ flux values, 73.1, 69.0, and 70.6, respectively. The number of storm days appears to reduce during these low solar activity years. Figure 7 in the work of Gonzalez et al. [1994] also depicts reduced number of storm days during low solar activity in sunspot cycle 21.

The storm days were binned into different solar flux levels using daily solar flux index, $F_{10.7}$, obtained from Space Weather Prediction Center (SWPC) of the National Oceanic and Space Administration (NOAA) (<http://www.swpc.noaa.gov/>). More details about the binning criteria is given in section 4. As described in section 3, the AE indices (<http://swdcwww.kugi.kyoto-u.ac.jp/>) were used to determine the occurrence of disturbed dynamo electric fields.

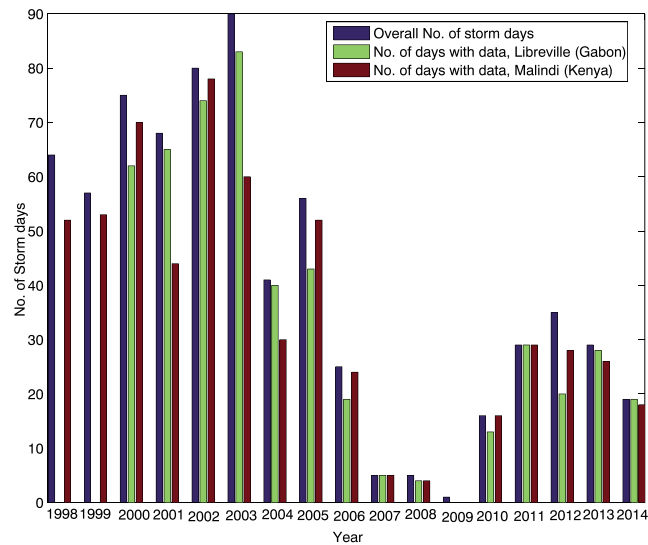


Figure 1. Distribution of number of storm days during 1998–2014. Blue, green, and brown bars represent the overall number of storm days, number of storm days with data over Libreville, and the number of storm days with data over Malindi, respectively.

The historical techniques that have been utilized for studying ionospheric irregularities include (i) ground-based ionosondes [Farley et al., 1970; Kelley and Hysell, 1991], (ii) scintillation of satellite signals in the VHF-UHF range [Fremouw et al., 1978; Paznukhov et al., 2012; Tanna et al., 2013], and (iii) satellite-borne topside sounders and in situ measurements [Kelley and Hysell, 1991; Hargreaves, 1992]. Techniques (i) and (ii) are suitable for irregularity scale sizes of the order of kilometers and hundreds of meters, respectively, while technique (iii) is suitable for nearly all the scale sizes [Abdu et al., 1998]. Recently, Aarons et al. [1996] and Pi et al. [1997] used the rate of change of total electron content (ROT) to study ionospheric irregularities. To identify and statistically present the smaller scale irregularities, Pi et al. [1997] defined the rate of change of TEC index (ROTI) by taking the standard deviation of ROT over a 5 min period. According to Zou and Wang [2009], large- and small-scale ionospheric irregularities at scale lengths of a few kilometers and ~400 m can be investigated simultaneously with the ROT and ROTI indices.

Based on availability of data resources, we used the ROTI index to represent ionospheric irregularities. The Receiver Independent Exchange (RINEX) data files used to extract the TEC which were in turn used to compute the ROTI index were obtained from the University NAVSTAR Consortium (UNAVCO) (<ftp://data-out.unavco.org/pub/rinex/>) data sites listed in Table 1. The method of extracting the vertical TEC (VTEC) from the RINEX data files in this study are similar to that found in Seemala and Valladares [2011]. The ROTI values for all satellites in view at the end of every 5 min (interval over which Pi et al. [1997] defined the ROTI) were averaged to obtain 5 min resolution data for a day. Before computing the ROTI, VTEC measurements with satellite elevation angle greater than 25° were considered in order to minimize the effects of multipath on the observations.

Table 1. GNSS Receivers Used in the Study^a

| Station | Code | Geographic | | | Usage in Model | |
|-------------------|------|------------|----------|----------------|----------------|-----|
| | | Lat (°N) | Lon (°E) | Modip Lat (°N) | Dev | Val |
| Libreville, Gabon | NKLG | 0.35 | 9.68 | -23.97 | X | |
| Masuku, Gabon | MSKU | -1.63 | 13.55 | -27.43 | | X |
| Yaounde, Cameroon | YAOU | 3.87 | 11.46 | -16.6 | | X |
| Malindi, Kenya | MAL2 | -2.99 | 40.19 | -24.92 | X | |
| Nairobi, Kenya | RCMN | -1.22 | 36.89 | -22.44 | | X |
| Eldoret, Kenya | MOIU | 0.29 | 35.29 | -19.870 | | X |
| Arusha, Tanzania | ARSH | -3.38 | 36.70 | -26.43 | | X |

^aX in columns 6 and 7 signify usage of data in model Dev and Val, respectively.

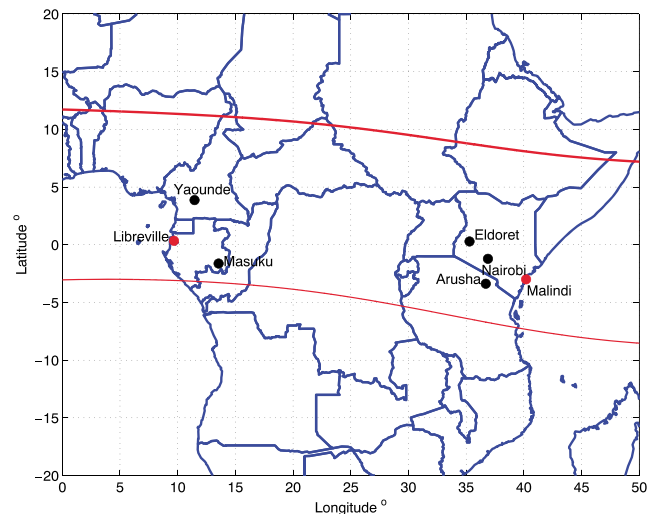


Figure 2. Map showing: (i) locations of Libreville, Nairobi, Malindi, Eldoret, Arusha, Yaounde, and Masuku. The red and black dots indicate data sites used for developing model and validation, respectively. (ii) The geomagnetic equator (thick red line) and the location of southern crest of equatorial ionization anomaly (thin red line).

The cutoff elevation angle 25° was arrived at after observing some plots of azimuth-elevation angle for all the satellites on some days. The azimuth-elevation angle plots (not shown here) for some of the stations mostly indicated that, at some azimuths, the lowest elevation angle over which satellites could be viewed were slightly above 20° .

The model that was developed over Malindi was validated with data over Nairobi, Eldoret, and Arusha. The model over Libreville was validated with data over Yaounde and Masuku. The geographic distribution of the data sites used in this study for modeling and validation is shown in Figure 2. As it can be seen in the figure, the data sites used for validation are close and in the same time zone as the stations over which models were developed. At Libreville and Malindi, the local time (LT) is given by adding 1 and 3 to the universal time (UT), respectively. In Figure 2 the thick and thin red lines indicate the location of the geomagnetic equator and the 15°S magnetic latitude, respectively, while the red and black dots indicate the data sites for developing and validating the models, respectively. The 15°S magnetic latitude is a nominal location of the southern equatorial ionization anomaly peak. The summary of information about the data sites used is presented in Table 1. Columns 6 and 7 in the table present usage of data marked X over a station for model development (Dev) and model validation (Val), respectively.

3. Geomagnetic Disturbance Effect on Ionospheric Irregularities

The effect of a geomagnetic disturbance on ionospheric irregularities may be associated to changes induced on zonal electric fields. In the first case, as stated in section 1, the prompt penetration electric fields that result in eastward electric field during daytime could lead to occurrence of ionospheric irregularities on the night that follows. Note that ionospheric irregularities also occur at night over low-latitude regions during quiet geomagnetic conditions [Mungufeni et al., 2016].

In the second case, the disturbed dynamo electric fields and intensification of ring current during daytime both decrease vertical plasma drift [Aarons, 1991; Fejer and Scherliess, 1995]. These might cause inhibitions of ionospheric irregularities. Days during which there were daytime (10:00–17:00 LT) significant ring current intensification were identified when Dst remained ≤ -50 nT for about 3 h consecutively. Following Fejer and Scherliess [1995] and the later discussions of Abdu [1997], we considered occurrence of disturbed dynamo electric fields at epoch t during daytime (10:00–17:00 LT) when one of the four conditions in Table 2 was satisfied. In the table, the Δ , two vertical bars, and horizontal bar over AE denote the difference between two consecutive values, magnitude, and average AE value, respectively. Days dominated by epochs with occurrence of disturbed dynamo electric fields were termed as disturbed dynamo electric field days. In Table 2, a common feature to all the four conditions appears to be the high average AE , 2–4 h before t . The delay in time

Table 2. Criteria for Identifying Disturbed Dynamo Electric Fields

| Case | $\Delta AE(t)$ | $ \Delta AE(t) $ | $\overline{AE}(-4 < t < -2)$ | $\Delta AE(t - 1)$ |
|-------|----------------|------------------|------------------------------|--------------------|
| (i) | ≤ 150 | | ≤ 300 | ≥ 150 |
| (ii) | | ≤ 150 | ≥ 200 | |
| (iii) | ≤ -125 | | ≥ 125 | |
| (iv) | | ≤ 150 | ≥ 175 | ≤ -125 |

might correspond to the disturbance wind dynamo propagation time to low latitudes after Joule heating at high latitudes by auroral current (evidenced by high average *AE*).

In order to illustrate the impact of geomagnetic disturbance on inhibition of ionospheric irregularities, we analyzed ROTI data over Malindi for 109 geomagnetically disturbed days during 2000 and 2001. These are high solar activity years which usually experience ionospheric irregularities. The ROTI data were examined for the existence of inhibition, while the *Dst* and *AE* indices of the corresponding days were examined for the existence of daytime intensification of ring current and disturbed dynamo electric fields, respectively. It is already well known that ionospheric irregularities in low-latitude regions mostly occur after sunset [Andrzej *et al.*, 2004]. In line with this information, we suggested that for a particular day, inhibition of ionospheric irregularities occurs when the mean of ROTI values during the day exceeds that of the night values according to the following equation,

$$MDR + 2\sigma \geq MNR, \tag{1}$$

where *MDR*, σ , and *MNR* represent the mean of ROTI values during 11:00–16:00 LT, the standard deviation of ROTI values during 11:00–16:00 LT, and mean of ROTI values during 20:00–03:00 LT, respectively. As we do not have a priori information about inhibition of ionospheric irregularities, equation (1) actually gives nights with no or low ionospheric irregularities. Since nonoccurrence or low occurrence of irregularities on some nights might be due to inhibition, we generalize in the mean time that this equation gives inhibition nights. Some few high variations of ROTI values at night might make the nighttime mean ROTI high. In order to balance this effect, fairly high error term (2σ) was added to daytime mean ROTI. Therefore, the high nighttime mean ROTI values due to some few high nighttime ROTI values might have not limited identification of inhibitions.

The result of our analysis revealed that a total of 50 nights had inhibitions. The mean ROTI value during the nights was 0.213 total electron content unit, $1TECU = 10^{16} \text{ el m}^{-2} \text{ (TECU)/Min}$. The percentages of inhibitions predicted by daytime intensification of ring current, disturbed dynamo electric fields, and either intensification of ring current or disturbed dynamo electric fields are presented in Table 3. The table also presents the percentages of occurrence of daytime ring current intensification, disturbed dynamo electric fields, and either intensification of ring current or disturbed dynamo electric field occurring simultaneously with inhibitions. The third column of Table 3 reveals that observations of ring current intensification, disturbed dynamo electric fields, and either intensification of ring current or disturbed dynamo electric field does not always mean inhibition of ionospheric irregularities. In section 4, we show that this problem can partly be solved. Based on the fairly good predictions of inhibitions of ionospheric irregularities by either daytime ring current intensification or disturbed dynamo electric fields, they were used to infer inhibitions of ionospheric irregularities. The days for which there were no inhibitions predicted were assumed to have ionospheric irregularities. Similar observation of inhibitions of ionospheric irregularities during geomagnetic storms was reported by Singh *et al.* [2004]. Out of the 50 storms during which they studied scintillation activities over the Indian low-latitude region, no scintillation activities were recorded during 28 of them. They stated that scintillations occur at arbitrary times and they may last for < 30 min. Ngwira *et al.* [2013] observed over the African low-latitude region

Table 3. Statistics of Ionospheric Irregularity Inhibitions During 2000–2001 Over Malindi

| Geomagnetic Disturbance Phenomena | Inhibitions Predicted (%) | Correct Predictions of Inhibitions (%) |
|---|---------------------------|--|
| Ring current | 62 | 62 |
| Disturbed dynamo electric fields | 56 | 61 |
| Either ring current or disturbed dynamo electric fields | 80 | 57 |

the occurrence of ionospheric irregularities during the moderate storm of 13–15 September 2014. Some stations experienced ionospheric irregularities while others did not, depending on the LT at the station when ring current intensified occurred.

4. Data Organization

One of the factors necessary for the occurrence of ionospheric irregularities is the existence of strong electron density gradients [Rastongi, 1980]. In low latitude and midlatitude, this is usually created when neutral atmospheric constituents absorb solar extreme ultraviolet (EUV) and X-ray radiation. The $F_{10.7}$ flux is well correlated with X-ray and EUV radiations [Davies, 1989]. Therefore, based on the daily $F_{10.7}$ flux values, the ROTI data for each of the stations over which models were developed were grouped into two bins of medium solar flux (MSF) and high solar flux (HSF). Bins of medium and high solar flux levels with $F_{10.7}$ value ranges as $80 \leq F_{10.7} \leq 120$ and $F_{10.7} > 120$, respectively, were only considered since ionospheric irregularities occur mostly during these flux levels [Mungufeni et al., 2016]. Another reason for only considering medium and high solar flux levels might be the low number of geomagnetic disturbances during these levels (see section 2). We would not have adequate data to represent occurrence of ionospheric irregularities during low solar flux level.

The data in each of the solar flux bins were grouped according to the 12 months of a year. Furthermore, the data in a month were sorted according to whether it was inhibition or occurrence of ionospheric irregularity day as inferred from *Dst* and *AE* indices. The lower quartile of all data in a month with inhibitions were determined at every epoch to represent monthly data with inhibitions at 5 min resolution. Monthly data with ionospheric irregularities at the same data resolution were determined in a similar way from all data in a month with ionospheric irregularities by taking upper quartiles. By taking the lower quartile, we eliminated the impact of data with ionospheric irregularities generated in the bin that contains data with inhibitions, while taking the upper quartile eliminated the impact of data with inhibitions. The monthly data were then arranged in LT bins. Since ionospheric irregularities mostly occur at night, the LT bins ranged from 18:00 to 06:00. The LT bins had resolution of 1 h. The median of ROTI values in the local time bins were then determined to represent hourly ROTI values.

The number of days with data in a month used to determine the monthly data may affect the performance of the model in that month. Figures 3a and 3b present the number of days used to determine the monthly ROTI over Libreville and Malindi, respectively. The black, green, red, and blue bars represent the number of days in high solar flux level with ionospheric irregularities (H irregularities), medium solar flux level with ionospheric irregularities (M irregularities), high solar flux level with inhibitions (H inhibitions), and medium solar flux with inhibitions (M inhibitions), respectively. Figures 3a and 3b shows that the months of October and November lacked data to represent medium solar flux level with occurrence of irregularities over Libreville and Malindi, respectively. This lack of data in these months is also reflected in Figures 3c and 3d, which presents the 5 min resolution monthly ROTI (as described in the previous paragraph) over Libreville and Malindi, respectively. In Figures 3c and 3d, black, green, red, and blue lines present the monthly ROTI in high solar flux level with ionospheric irregularities, medium solar flux level with ionospheric irregularities, high solar flux level with inhibitions, and medium solar flux with inhibitions, respectively. The zero values of ROTI in the months of October and November over Libreville and Malindi, respectively, in medium solar flux level with occurrence of irregularities signify lack of data. In such conditions and those for which the number of days is less than 5, we might not expect very good performance of the models.

5. The Model

The ionospheric irregularity strength (hourly ROTI) as a function of LT (t), month (m), solar flux (F), and storm effect (E) was expressed as a tensor product as follows [Abdu et al., 2003; Iyer et al., 2006; Mungufeni et al., 2015]:

$$P(t, m, F, E) = \sum_{i=1}^{12} \sum_{j=1}^{12} \sum_{k=1}^2 \sum_{l=1}^3 a_{i,j,k,l} N_{i,4}(t) N_{j,2}(m) N_{k,2}(F) N_{l,2}(E), \quad (2)$$

where $N_{i,4}(t)$ is a cubic B-spline of order four applied to LT dependence (t). The $N_{j,2}(m)$, $N_{k,2}(F)$, and $N_{l,2}(E)$ are cubic B-splines of order two applied to monthly or seasonal (m), solar flux (F), and storm effect (E) dependencies, respectively. Because of the rapid changes in occurrence of ionospheric irregularities with LT,

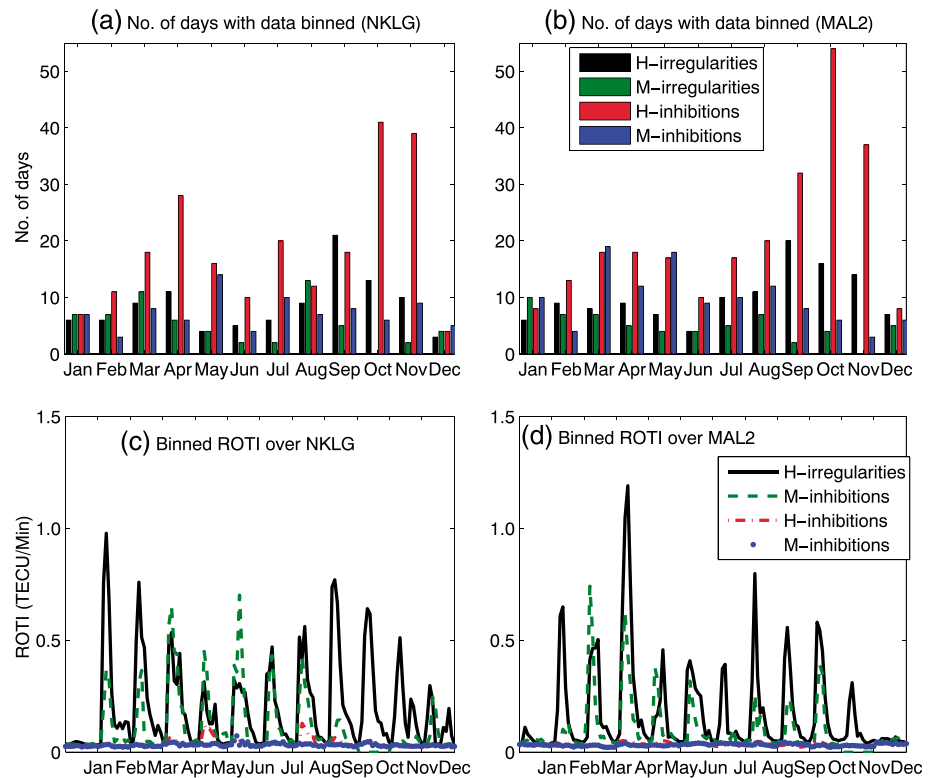


Figure 3. Number of days used to obtain monthly ROTI over (a) NKLG and (b) MAL2. The black, green, red, and blue bars represent the number of days in HSF with ionospheric irregularities (H irregularities), MSF with ionospheric irregularities (M irregularities), HSF with inhibitions (H inhibitions), and MSF with inhibitions (M inhibitions), respectively. (c, d) The monthly ROTI with 5 min resolution that were used to develop models over NKLG and MAL2, respectively. The black, green, red, and blue lines present the monthly ROTI in: H irregularities, M irregularities, H inhibitions, and M inhibitions, respectively.

especially after sunset, a higher order ($N_{i,4}(t)$) cubic B-spline was used to represent LT dependence [Scherliess and Fejer, 1999]. The coefficients $a_{i,j,k,l}$ were determined by the weighted least squares fit to the binned data (Figures 3c and 3d). The various nodes were determined in a similar way as in Scherliess and Fejer [1999], Abdu et al. [2003], Iyer et al. [2006], and Mungufeni et al. [2015]. For a day, 12 local time nodes were used and distributed between 18:00 and 06:00. For simple interpolation between months, seasonal/monthly nodes were placed at the fifteenth day of each month. The solar flux nodes used to represent solar activity in each month were determined by averaging the daily values during the storms that occur in the respective month. The storm effects of inhibited ionospheric irregularity (IOII) and occurrence of ionospheric irregularity (OII) were represented by the numbers 1 and 2, respectively.

6. Comparison of Model Results With Observed Data

The observed hourly ROTI over Libreville and Malindi during the storm days in the year 2000 have been presented simultaneously with the corresponding modeled values in Figure 4. This is to show that the models developed over these stations were able to reproduce fairly well the data which were binned and used in their development. For purposes of showing clearly inhibitions and occurrence of ionospheric irregularities, high solar activity year 2000 when high levels of occurrence of ionospheric irregularities was expected was used. Figures 4a and 4b present the observed and the modeled ROTI, respectively, over Libreville, while Figures 4c and 4d present the observed and modeled ROTI, respectively, over Malindi. For clarity purposes, some of the dates on the horizontal axis are not indicated. In Figures 4–9 white spaces indicate missing data, while the color bar ranges from blue (low ROTI) to red (high ROTI). In this section, we categorized nights when the hourly ROTI values were all < 0.3 TECU/Min as inhibition nights. Note that in section 3, the mean value of ROTI during nights with inhibitions was found to be about 0.213 TECU/Min.

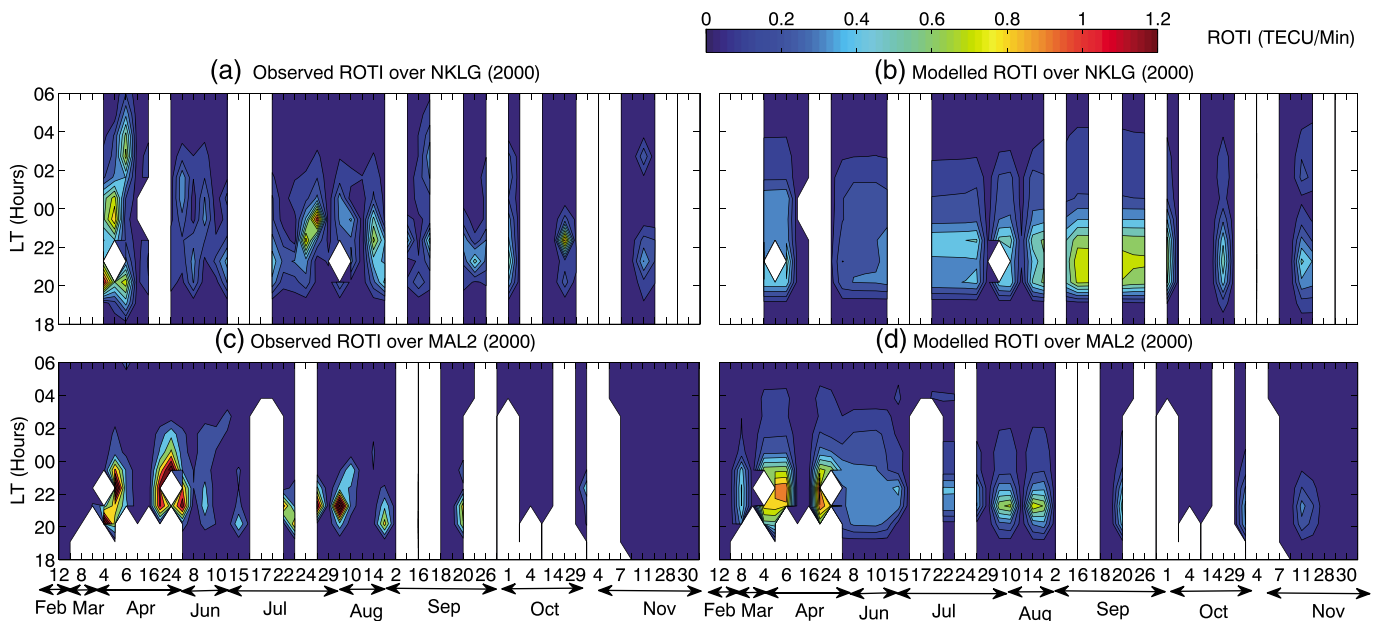


Figure 4. (a, c) Observed and (b, d) modeled hourly ROTI over NKLG and MAL2 on the nights of some storm days in the year 2000. Figures 4a and 4b are for NKLG, while Figures 4c and 4d are for MAL2. The color bar ranges from blue (low ROTI) to red (high ROTI). The white spaces indicate missing data.

It can be observed in Figure 4 that ionospheric irregularities mostly occur starting from about 20:00 LT to about 02:00 LT. On the days when there is no inhibitions, the equatorial *F* layer rises to higher altitudes after sunset. This occurs due to the enhanced eastward electric field, known as the prereversal enhancement [Li *et al.*, 2009]. When the *F* layer has risen to an altitude where the ion-neutral collision frequency is small, the local Rayleigh-Taylor (RT) instability becomes susceptible to triggering. This condition is favorable for the development of irregularities [Li *et al.*, 2009]. Considering a particular date on Figure 4 when there is data over both stations, the inhibitions or occurrence of ionospheric irregularities in most cases are seen simultaneously over both stations. Due to the different local times at the stations, the strengths of the observed ionospheric irregularities over both stations on same date are not always the same [Valladares *et al.*, 2004].

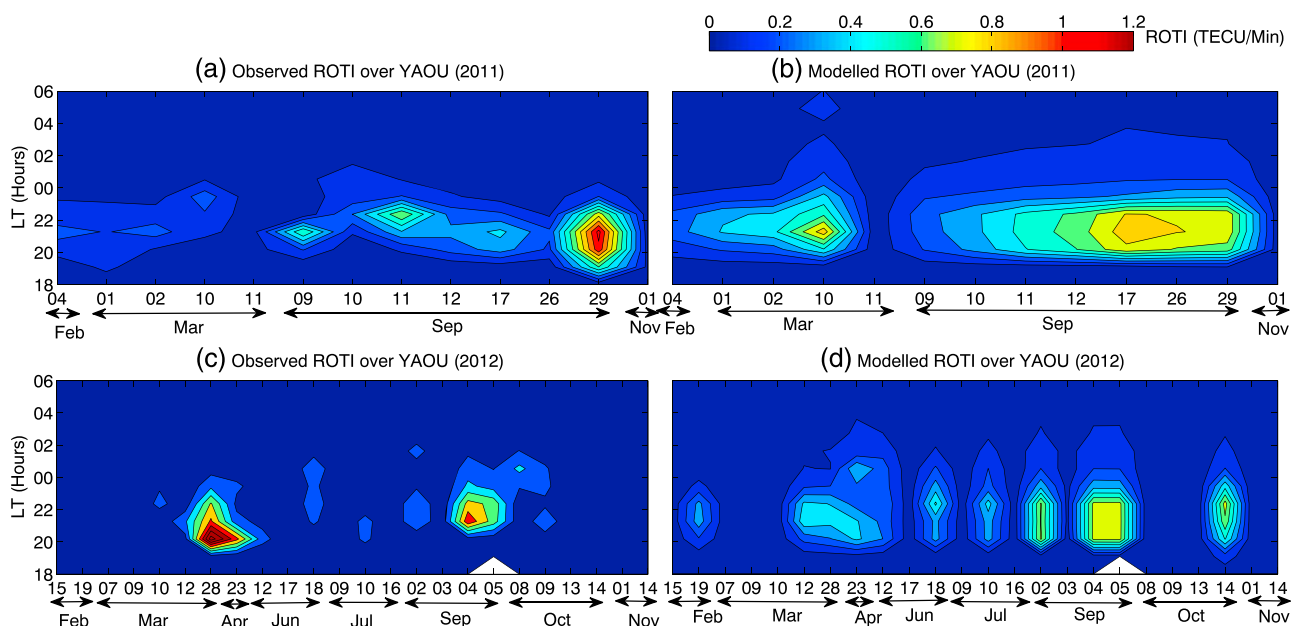


Figure 5. (a, c) Observed and (b, d) modeled hourly ROTI over YAOU on nights of some storm days during 2011–2012. The color bar ranges from blue (low ROTI) to red (high ROTI). The white spaces indicate missing data.

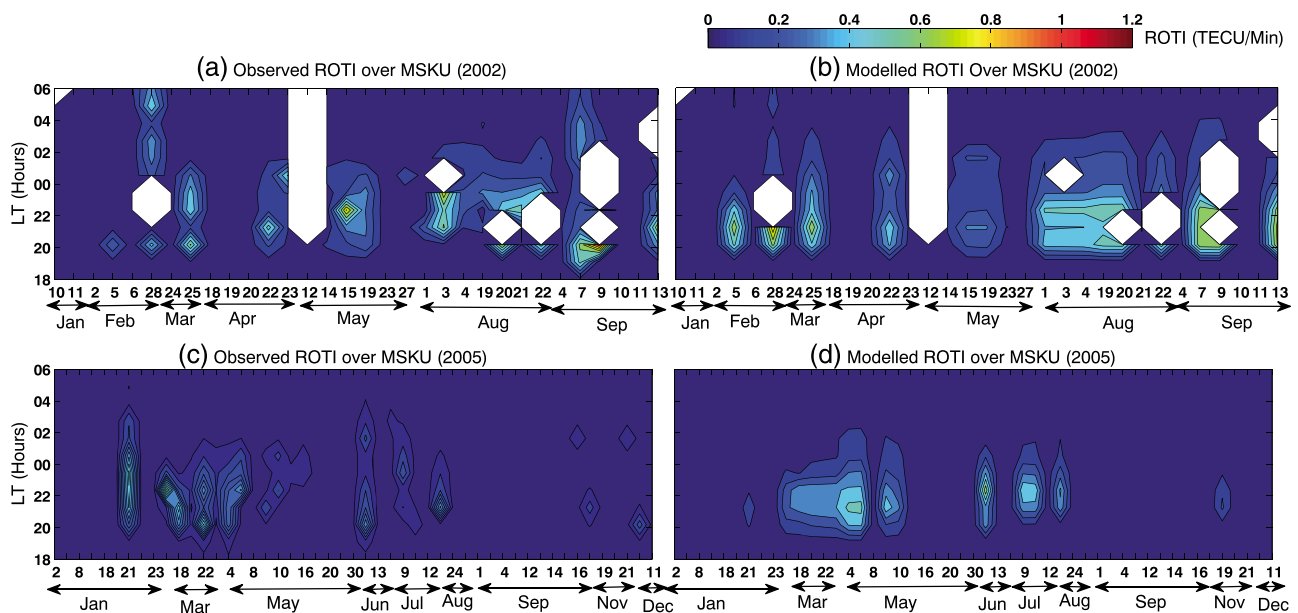


Figure 6. (a, c) Observed and (b, d) modeled hourly ROTI over MSKU on nights of some storm days during 2002 and 2005. The color bar ranges from blue (low ROTI) to red (high ROTI). The white spaces indicate missing data.

During most of the days, the models try to reproduce the inhibitions and occurrence of ionospheric irregularities depicted by the observed data in Figures 4a and 4c. However, there are few cases when the observed data show either inhibition or occurrence of ionospheric irregularities, but the modeled data do not capture them. Over Libreville, typical examples are on 22 July, 16 September, while over Malindi, the examples are on 8 March, 8 and 10 June, 14 August, and 11 November. The observed discrepancies might have been due to the fact that data of the year 2000 was only part of data used in model development. So, the model might have captured broader or general features of inhibitions and occurrence of ionospheric irregularities and averaged or smoothed out features of the year 2000.

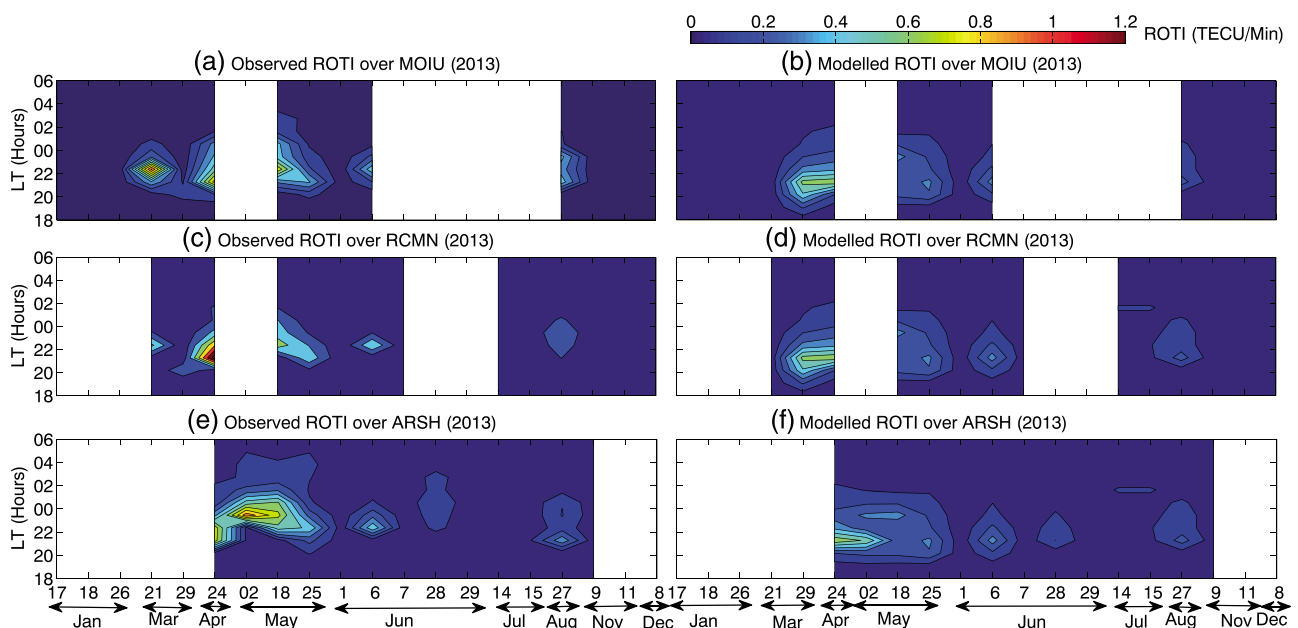


Figure 7. (a, c, and e) Observed hourly ROTI over MOIU, RCMN, and ARSH, respectively, during 2013 and (b, d, and f) the modeled ROTI over the same stations in that order during the same period. The color bar ranges from blue (low ROTI) to red (high ROTI). The white spaces indicate missing data.

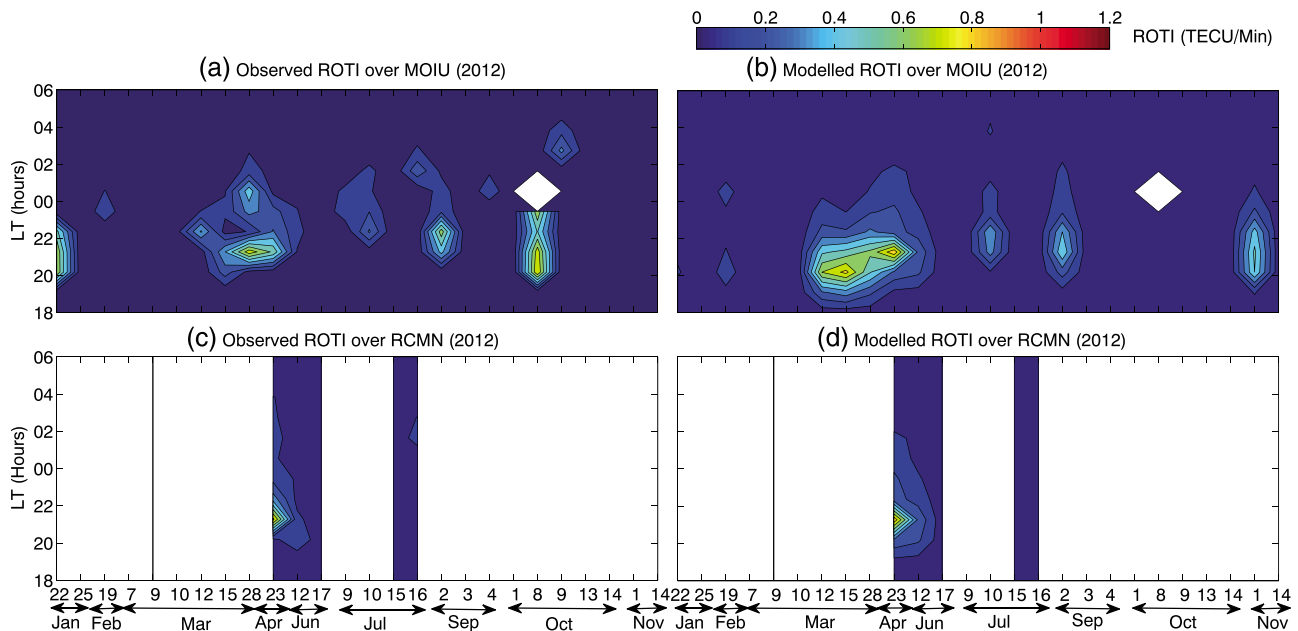


Figure 8. (a, c) Observed hourly ROTI over MOIU and RCMN, respectively, during 2012 and (b, d) the modeled ROTI over the same stations in that order during the same period. The color bar ranges from blue (low ROTI) to red (high ROTI). The white spaces indicate missing data.

The real ability of the developed models to reproduce the pattern of occurrence of ionospheric irregularities during disturbed geomagnetic conditions was ascertained by comparing their output with observed data over stations whose data were not used in the model development. In sections 6.1 and 6.2, we present and discuss the results for the validation of the model developed over Libreville and Malindi, respectively.

6.1. Validation of Libreville Model

First, the model over Libreville was validated with data over Yaounde which is at straight line distance of about 450 km. The results are presented in Figure 5. Figures 5a and 5b present the observed and the modeled ROTI, respectively, during the storm days indicated on the horizontal axis in 2011, while Figures 5c and 5d present the observed and the modeled ROTI, respectively, for the year 2012. The station at Yaounde was operational since 2011. It only had fairly adequate data during 2011 and 2012.

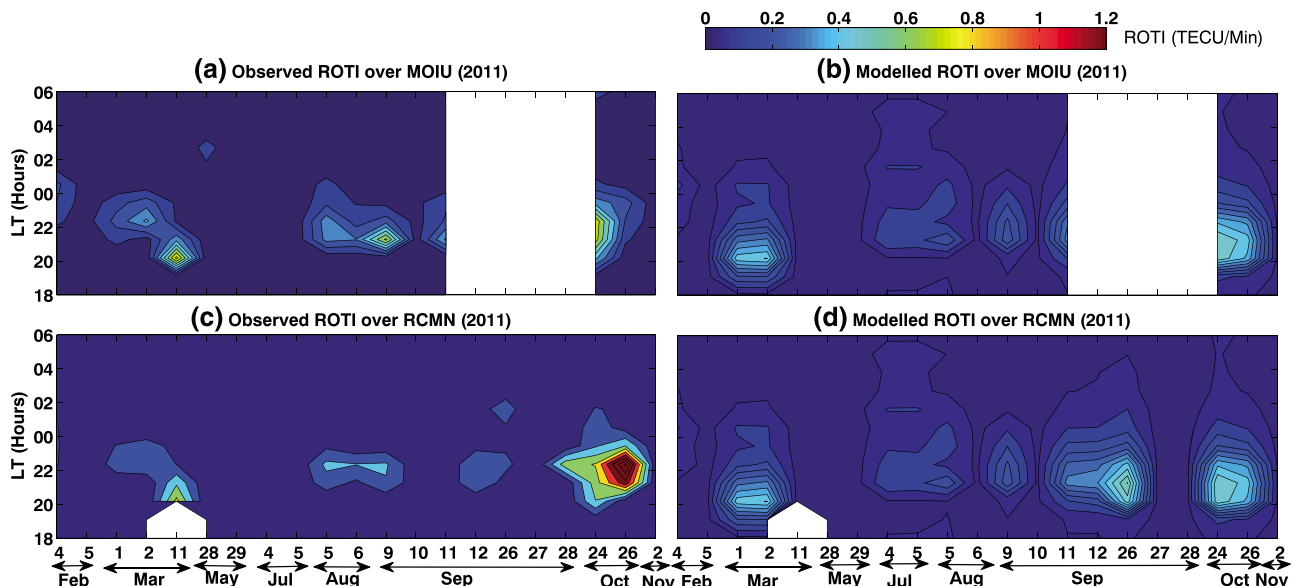


Figure 9. Similar to Figure 8 but for the year 2011.

Similar to the earlier observation made over Malindi and Libreville, occurrence of ionospheric irregularities mostly starts from about 20:00 LT to about 02:00 LT. During most of the days, the model tries to capture the inhibitions and occurrence of irregularities depicted by the observed data in Figures 5a and 5c. However, there are also cases when the model did not perform well in predicting the inhibitions and occurrence of ionospheric irregularities. For instance, out of the 37 nights presented in Figure 5, eight nights (In 2011, 1, 2, and 10 March, while in 2012, 19 February, 18 June, 10 July, 2 September, and 14 October) showed cases of the model not capturing the inhibitions and occurrence of ionospheric irregularities in the observed data. The poor performance of the model during these dates might be due to (i) the inability to perfectly predict inhibitions on the storm days used for validation (correct probability being about 0.8), (ii) the predicted inhibitions always may not be accompanied by actual inhibitions on the storm days (correct probability being about 0.57). These problems, which were partly solved in section 4, might originate from lack of representation of other factors such as meridional winds in the prediction of inhibitions. A meridional wind, whether or not related to disturbed conditions, can modify the low-latitude ionospheric response to disturbance dynamo electric field [Abdu, 1997]. Unfortunately, there seem to be no record of neutral wind data measurements over the African low-latitude region at the moment. Some of the discrepancies seem to be related to inadequate number of days that constitute monthly ROTI used in model development over Libreville (see some cases in June, July, and October in Figure 3a).

Second, the model over Libreville was validated with data over Masuku which is approximately at straight line distance of about 510 km. The station was operational during 2001–2007. The data of the years 2002 (HSF) and 2005 (MSF) were used. The results are presented in Figure 6 which is similar to Figure 5. The observed and the modeled ROTI data have exhibited features similar to that over Yaounde which were discussed previously. Though there is overwhelming evidence that the model tries to imitate the inhibitions and occurrences of ionospheric irregularities over Masuku, there still exists discrepancies between the observed and the modeled data during some dates. For example, in 2002, on 5 February, 1, 4, and 21 August, while in 2005, on 21 January, 21 and 23 March, 9 May, and 23 June, 9 and 11 July.

6.2. Validation of Malindi Model

The model that was developed using data over Malindi was validated with data over Eldoret, Nairobi, and Arusha. These stations are on straight line distances of about 380, 430, and 680 km, respectively, from Malindi. In order to compare the ROTI values over the three stations during the same nights, the data over the three stations were plotted in panels that form a column as shown in Figures 7–9. Figures 7a and 7b, 7c and 7d, and 7e and 7f present the data over Eldoret, Nairobi, and Arusha, respectively, during 2013. For each station, the panels represent observed and modeled data, respectively. There were no data archived at Arusha for the years 2011 and 2012. Therefore, Figures 8 and 9 only present the data over Eldoret (a and b) and Nairobi (c and d). In most cases when there is simultaneous data over two (e.g., in 2011 and 2012) or three (e.g., in 2013) stations on a particular date, similar responses of either inhibition or occurrence of irregularity are seen all over the stations. Figures 7–9 show that in most cases the model tries to reproduce inhibition or occurrence of irregularities depicted by the observed data. Prominent exceptions can be seen on 11 March, 5 August, and 26 September in 2011, 22 January, 8 October, and 1 November in 2012, and 21 and 29 March, 18 May, and 27 August in 2013.

7. Verification of Prediction Skills of Models

In order to establish how well the modeled ROTI values correspond to the observed, correlation analysis was performed. Figures 10a–10e present scatterplots of modeled ROTI values against observed ROTI values over Eldoret, Nairobi, Arusha, Yaounde, and Masuku, respectively. In the figure, on the top right of each panel, the corresponding correlation coefficient, r , is presented. The data used in Figures 10a–10e correspond to those in Figures 5–9. It can be seen from the panels that most of the correlations are strong positive relations ($r \geq 0.5$). However, the correlation between the Modeled and observed ROTI over Eldoret is moderate positive ($0.3 \leq r < 0.5$). This is the farthest station among those that were used for validations. Generally, as the distance between the station used for validation and that used for model development increases, r decreases. The degradation in the correlations as distance from where models are developed increases may be due to changes of physical conditions that generate ionospheric irregularities.

In addition to the correlation analysis, we also analyzed the errors (difference between the observed and the modeled data) when using the models to estimate the ROTI over Yaounde, Masuku, Eldoret, Nairobi,

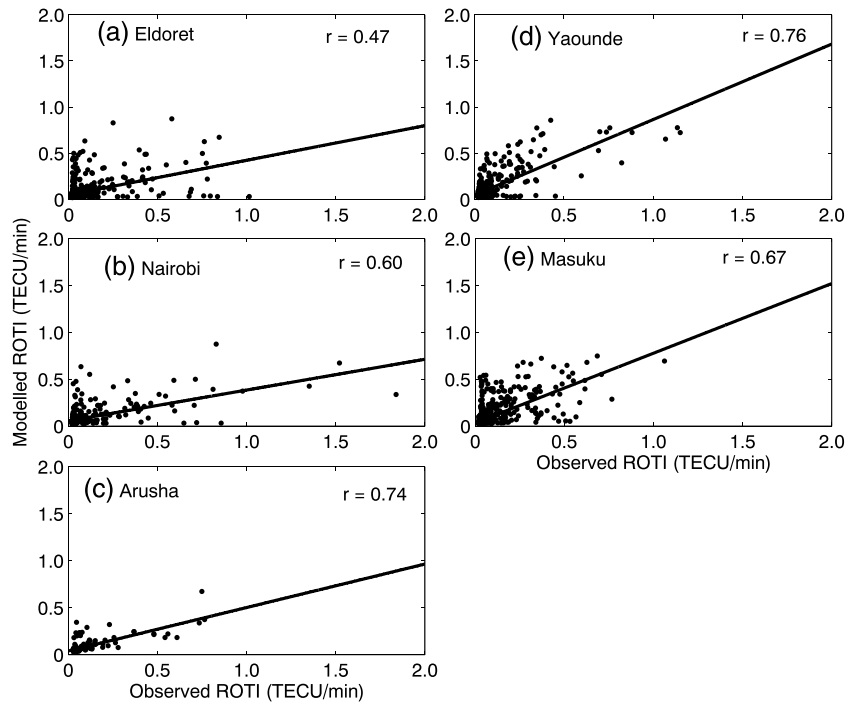


Figure 10. Scatterplots of modeled ROTI against observed ROTI over (a) Eldoret, (b) Nairobi, (c) Arusha, (d) Yaounde, and (e) Masuku. Top right of the panels show the corresponding correlation coefficient, r . The data plotted correspond to those in Figures 5–9.

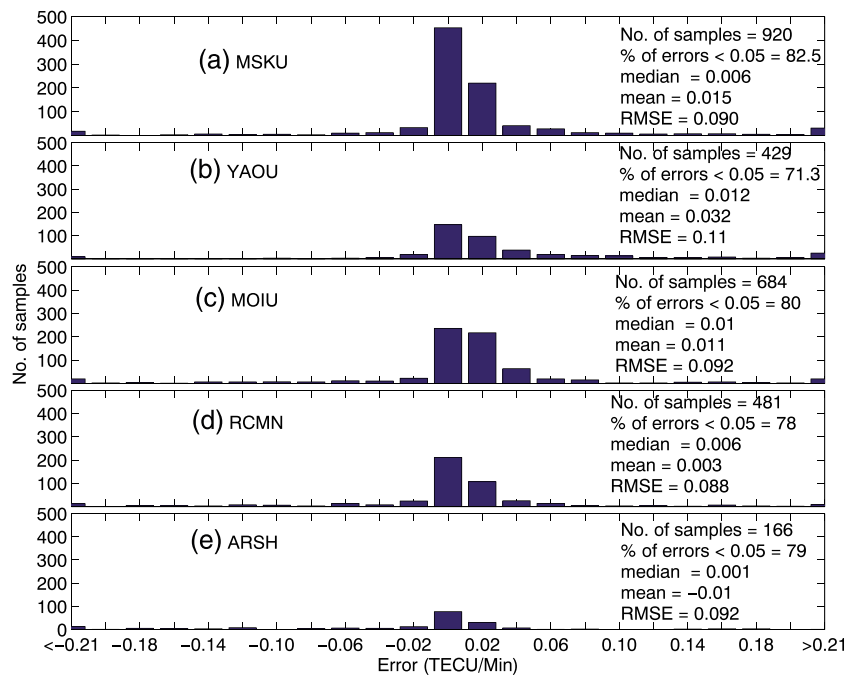


Figure 11. Frequency distribution of the error (difference between modeled and observed ROTI values) over (a) MSKU, (b) YAOU, (c) MOIU, (d) Nairobi, and (e) ARSH. The errors correspond to the data that were plotted in Figures 5–9.

and Arusha. The number of errors during validations over these stations has been determined on intervals of 0.02 TECU/Min that were centered on -0.2 , -0.18 , -0.16 , ... 0.2 . The results are presented in Figures 11a–11e. On the right of each panel in Figure 11 are shown the number of samples, percentage of the number of errors < 0.05 TECU/Min, median of the error values, the mean of the error values, and the root-mean-square error (RMSE). Clearly, the mean of the errors over all the stations shows that the errors are random in nature (mean ~ 0). The percentages of the number of errors < 0.05 TECU/Min for the validations over all the stations are all above 70%. This is an indication that to a great extent, the models are capable of reproducing the inhibitions and occurrence of ionospheric irregularities during geomagnetic conditions within the coverage of the stations that were used for validation. The lowest percentage (71.3%) recorded during the validation over Yaounde might be associated to its modip latitude separation from Libreville. The modip latitude separation of Yaounde and Masuku from Libreville are 7.37° and 3.46° , respectively. The mechanism that generate irregularities over Yaounde might vary slightly from that over Libreville due to this modip latitude separation. Most of the RMSE are < 0.1 TECU/Min, except for the validation over Yaounde. Considering that the observed ROTI values can be up to > 1 TECU/Min, RMSE values < 0.1 TECU/Min suggest fairly good performance of the models.

8. Conclusions

Empirical models of occurrence of ionospheric irregularities over low-latitude African region during disturbed geomagnetic conditions have been developed. The model over Libreville was validated with data over Yaounde and Masuku, which are at straight line distances of about 450 and 510 km, respectively, from Libreville, while the model over Malindi was validated with data over Arusha, Nairobi, and Eldoret, which are at straight line distances of about 380, 430, and 680 km, respectively, from Malindi. The correlation coefficients between modeled and observed ROTI over the stations where validations were conducted ranged from 0.47 to 0.76. The RMSE values for the validations were mostly < 0.1 TECU/Min. During validations of the models, the percentages of the number of errors < 0.05 TECU/Min were all $> 70\%$. Based on the stated validation results, the models reproduced fairly well the inhibitions and occurrences of ionospheric irregularities during disturbed geomagnetic conditions over the stations where validations were conducted. The models emulated these patterns in the various seasons during medium and high solar activity conditions (see Figures 4–9). To improve the performance of these models, the problems of inability to perfectly predict inhibitions and the predicted inhibitions not always occurring need to be addressed. This might be achieved by incorporating information on meridional winds in the prediction of inhibitions. The inadequate number of days in some cases used to derive monthly ROTI which in turn were used in model development might be another limitation of the current models. For practical applications, the models developed in the current study will be combined in future with the geomagnetically quiet time model [Mungufeni et al., 2015].

Acknowledgments

P. Mungufeni acknowledges the South African National Space Agency (SANSA) for hosting him at the Space science directorate during April–June 2015, where the idea of the study was conceived. He acknowledges the International Science Program (ISP), for the financial support. He is also thankful to ICTP for hosting him as Junior associate of the center during 2 May to 2 July 2016. The final draft of the manuscript was written during this period under the guidance of the head of T/ICT4D laboratory of ICTP, S. M. Radicella. J.B. Habarulema's contribution has been partly supported by the South Africa's National Research Foundation (NRF) grant 90331. The data used in this study were obtained from (i) <ftp://data-out.unavco.org/pub/rinex/>, (ii) <http://swdwww.kugi.kyoto-u.ac.jp/>, and (iii) <http://www.swpc.noaa.gov/>.

References

- Aarons, J. (1985), Construction of a model of equatorial scintillation intensity, *Radio Sci.*, 20(3), 397–402.
- Aarons, J. (1991), The role of the ring current in the generation or inhibition of equatorial *F* layer irregularities during magnetic storms, *Radio Sci.*, 26(4), 1131–1149.
- Aarons, J., M. Mendillo, and R. Yantosca (1996), GPS phase fluctuations in the equatorial region during the MISETA 1994 campaign, *J. Geophys. Res.*, 101(12A), 26,851–26,862.
- Abdu, M. A. (1997), Major phenomena of the equatorial ionosphere-thermosphere under disturbed conditions, *J. Atmos. Sol. Terr. Phys.*, 59(13), 1505–1519.
- Abdu, M. A., J. H. A. Sobral, I. S. Batista, V. H. Rio, and C. Medina (1998), Equatorial spread-*F* occurrence statistics in the American longitudes: Diurnal, seasonal and solar cycle variations, *Adv. Space Res.*, 22(6), 851–854.
- Abdu, M. A., J. R. Souza, I. S. Batista, and J. H. A. Sobral (2003), Equatorial spread *F* statistics and empirical representation for IRI: A regional model for the Brazilian longitude sector, *Adv. Space Res.*, 31(3), 703–716.
- Akasofu, S. (2007), *Exploring the Secrets of the Aurora*, Springer, Alaska.
- Anderson, D. N., B. Reinisch, C. Valladare, J. Chau, and O. Veliz (2004), Forecasting the occurrence of ionospheric scintillation activity in the equatorial ionosphere on a day-to-day basis, *J. Atmos. Sol. Terr. Phys.*, 66, 1567–1572.
- Andrzej, W. W., A. Lucilla, and M. Massimo (2004), Ionospheric irregularities, scintillation and its effect on systems, *Acta Geophys. Pol.*, 52(2), 237–249.
- Benestad, E. K. (2006), *Solar Activity and Earth's Climate*, Springer, Oslo, Norway.
- Blanc, M., and A. D. Richmond (1980), The ionospheric disturbance dynamo, *J. Geophys. Res.*, 45(A4), 1669–1686.
- DasGupta, A., A. Maitra, and S. K. Das (1985), Post-midnight equatorial scintillation activity in relation to geomagnetic disturbances, *J. Atmos. Sol. Terr. Phys.*, 47(8–10), 911–916.
- Davies, K. (1989), *Ionospheric Radio*, Inst. Eng. and Technol., London.
- de Paula, E. R., et al. (2007), Characteristics of the ionospheric *F*-region plasma irregularities over Brazilian longitudinal sector, *Indian J. Radio Space Phys.*, 36, 268–277.
- Farley, D. T., B. B. Balsley, R. F. Woodman, and J. P. McClure (1970), Equatorial spread *F*: Implications of VHF radar observations, *J. Geophys. Res.*, 75(34), 7199–7216.

- Fejer, B. G., and L. Scherliess (1995), Time dependent response of equatorial ionospheric electric fields to magnetospheric disturbances, *Geophys. Res. Lett.*, *22*(7), 851–854.
- Fremouw, E. J. R. L., Leadabrand, R. C., Livingston, M. D., Cousins, C. L., Rino, B. C., Fair, and R. A. Long (1978), Early Results from the DNA Wideband satellite experiment—Complex-signal scintillation, *Radio Sci.*, *13*(1), 167–187.
- Gonzalez, W. D., J. A. Joselyn, Y. Kamide, H. W. Kroehl, G. Rostoker, B. T. Tsurutani, and V. M. Vasyliunas (1994), What is a geomagnetic storm?, *J. Geophys. Res.*, *99*(A4), 5771–5792.
- Hargreaves, J. K. (1992), *The Solar-Terrestrial Environment*, Cambridge Univ. Press, Cambridge, U. K.
- Iyer, K. N., J. R. Souza, B. M. Pathan, M. A. Abdu, M. N. Jivani, and H. P. Joshi (2006), A model of equatorial and low latitude VHF scintillation in India, *Indian J. Radio Space Phys.*, *35*, 98–104.
- Kallenrode, M. (2003), *Space Physics: An Introduction to Plasmas and Particles in the Heliosphere and Magnetospheres*, Springer, Berlin, and Osnabruck, Germany.
- Kelley, M. C., and D. L. Hysell (1991), Equatorial spread-F and neutral atmospheric turbulence: A review, *J. Atmos. Terr. Phys.*, *53*(8), 695–708.
- Li, G., B. Ning, L. Liu, W. Wan, and J. Y. Liu (2009), Effect of magnetic activity on plasma bubbles over equatorial and low-latitude regions in East Asia, *Ann. Geophys.*, *27*, 303–312.
- Moldwin, M. (2008), *An Introduction to Space Weather*, Cambridge Univ. Press, New York.
- Muella, M. T. A. H., E. R. de Paula, I. J. Kantor, L. F. C. Rezende, and P. F. Smorigo (2009), Occurrence and zonal drifts of small-scale ionospheric irregularities over an equatorial station during solar maximum—Magnetic quiet and disturbed conditions, *Adv. Space Res.*, *43*, 1957–1973.
- Mungufeni, P., E. Jurua, J. B. Habarulema, and S. K. Anguma (2015), Modelling the probability of ionospheric irregularity occurrence over African low latitude region, *J. Atmos. Sol. Terr. Phys.*, *128*, 46–57.
- Mungufeni, P., J. B. Habarulema, and E. Jurua (2016), Trends of ionospheric irregularities over African low latitude region during quiet geomagnetic conditions, *J. Atmos. Sol. Terr. Phys.*, *138–139*, 261–267.
- Ngwira, C. M., G. K. Seemala, and J. B. Habarulema (2013), Simultaneous observations of ionospheric irregularities in the African low-latitude region, *J. Atmos. Sol. Terr. Phys.*, *97*, 50–57.
- Paznukhov, V. V., et al. (2012), Equatorial plasma bubbles and L-band scintillations in Africa during solar minimum, *Ann. Geophys.*, *30*, 675–682.
- Pi, X., A. J. Mannucci, U. J. Lindqwister, and C. M. Ho (1997), Monitoring of global ionospheric irregularities using the worldwide GPS network, *Geophys. Res. Lett.*, *24*(18), 2283–2286.
- Rastongi, R. G. (1980), Seasonal variation of equatorial spread *F* in the American and Indian zones, *J. Geophys. Res.*, *85*(A2), 722–726.
- Sastri, J. H., K. B. Ramesh, and D. Karunakaran (1992), On the nature of substorm-related transient electric field disturbances in the equatorial ionosphere, *Planet. Space Sci.*, *22*, 95–103.
- Scherliess, L., and B. G. Fejer (1999), Radar and satellite global equatorial *F* region vertical drift model, *J. Geophys. Res.*, *104*(4A), 6829–6842.
- Schunk, W. R., and F. A. Nagy (2009), *Ionospheres: Physics, Plasma Physics, and Chemistry*, Cambridge Univ. Press, New York.
- Seemala, G. K., and C. E. Valladares (2011), Statistics of total electron content depletions observed over the South American continent for the year 2008, *Radio Sci.*, *46*, R55019, doi:10.1029/2011RS004722.
- Secan, J. A., R. M. Bussey, E. J. Fremouw, and S. Basu (1995), An improved model of equatorial scintillation, *Radio Sci.*, *30*(3), 607–617.
- Singh, R. P., R. P. Patel, and A. K. Singh (2004), Effect of solar and magnetic activity on VHF scintillations near the equatorial anomaly crest, *Ann. Geophys.*, *22*, 2849–2860.
- Tanna, H. J., S. P. Karia, and K. N. Pathak (2013), A study of L band scintillations during the initial phase of rising solar activity at an Indian low latitude station, *Adv. Space Res.*, *52*, 412–421.
- Valladares, C. E., J. Villalobos, R. Sheehan, and M. P. Hagan (2004), Latitudinal extensions of low-latitude scintillations measured with a network of GPS receivers, *Ann. Geophys.*, *22*, 3155–3175.
- Zou, Y., and D. Wang (2009), A study of GPS ionospheric scintillations observed at Guilin, *J. Atmos. Sol. Terr. Phys.*, *71*, 1948–1958.